Diagn Interv Radiol 2017; 23:199–205

HEAD AND NECK IMAGING

ORIGINAL ARTICLE

Discrepant lesion size estimated on T1- and fat-suppressed T2-weighted MRI: diagnostic value for differentiation between inflammatory pseudotumor and carcinoma of the nasopharynx

Hye Na Jung
Hyung-Jin Kim
Yi Kyung Kim
Mina Song
Ha Yeon Kim
Kyung Min Park
Jihoon Cha
Sung Tae Kim

PURPOSE
Nasopharyngeal inflammatory pseudotumor (NIPT) is hard to differentiate from infiltrating nasopharyngeal carcinoma (NPC) on conventional magnetic resonance imaging (MRI). The purpose of this study is to determine whether discrepant lesion sizes estimated on T1- and fat-suppressed T2-weighted images can help distinguish between NIPT and NPC.

METHODS
We retrospectively reviewed MRI data of histologically proven 14 NIPTs and 18 infiltrating NPCs. We measured the area of the lesion on contrast-enhanced T1-weighted, unenhanced T1-weighted, and fat-suppressed T2-weighted images by placing the largest possible polygonal region-of-interest within the lesion at the same level. Using lesion size measured on contrast-enhanced T1-weighted image as the reference, we calculated and compared area ratio of T1 (AR_{T1}) and area ratio of T2 (AR_{T2}) between NIPTs and NPCs. For validation, we also undertook a double-blinded study by two reviewers and assessed the diagnostic performance and interobserver agreement.

RESULTS
For NIPTs, AR_{T2} (median, 0.48; range, 0.18–0.97) was statistically significantly less than AR_{T1} (median, 1.01; range, 0.80–1.99), while these values were not significantly different for NPCs. The interobserver agreement in differentiating between NIPT and NPC was good, with a sensitivity of 93% and a specificity of 83%–94%.

CONCLUSION
In contrast to NPCs, NIPTs appear smaller on fat-suppressed T2-weighted images than on T1-weighted images. This discrepancy in the lesion size estimated on T1-weighted and fat-suppressed T2-weighted images may provide a simple and consistent way to differentiate between NIPTs and NPCs on conventional MRI.

Inflammatory pseudotumor (IPT) represents a group of heterogeneous inflammatory diseases of unknown etiology and has rarely been reported to involve the nasopharynx(1–8). Nasopharyngeal inflammatory pseudotumor (NIPT) has a propensity for invasion of the adjacent structures, such as the deep cervical spaces, skull base, and cranial nerves. This aggressive behavior of NIPT frequently makes it difficult to distinguish from true invasive tumors such as nasopharyngeal carcinoma (NPC) both clinically and radiologically, and the diagnosis usually relies on histologic examinations (2, 9–11). Early diagnosis of NIPT is critical for achieving a better clinical outcome by implementation of the appropriate treatment options, such as steroid administration and radiation therapy, as soon as possible (8).

By virtue of superb contrast resolution, magnetic resonance imaging (MRI) has been used as the imaging modality of choice to define the nature and extent of various lesions of the head and neck. Although the advanced MRI techniques, such as dynamic susceptibility contrast-enhanced MRI, magnetic resonance spectroscopy, and diffusion-weighted imaging, may help illuminate the non-neoplastic nature of IPT to better advantage (5, 12–14), the gross extent of the lesions can be more conveniently appreciated on conventional MRI (15). Of the known conventional MRI features of IPT, hypointensity on T2-weighted images has been reported to serve as an important clue to differentiate IPT from aggressive malignancies (2, 9). We hypothesize that hypointensity of NIPT on T2-weighted images would result in underestimation of the lesion size compared with T1-weighted images, while this discrepancy would not be apparent in cases of NPC, which appear hyperintense on T2-weight-

From the Department of Radiology and Center for Imaging Science (H.N.J., H.J.K. ✉ *hyungkim@skku.edu*, Y.K.K., M.S., H.Y.K., K.M.P., J.C., S.T.K.), Samsung Medical Center, Sungkyunkwan University School of Medicine, Seoul, Korea; the Department of Radiology (M.S.), Hanil General Hospital, Seoul, Korea.

Received 6 August 2016; revision requested 29 October 2016; revision received 16 November 2016; accepted 22 November 2016.

Published online 19 April 2017.
DOI 10.5152/dir.2017.16241

ed images. The fat saturation technique, which is routinely used for the T2-weighted images of the modern head and neck MRI, may exaggerate this discrepancy for NIPTs, because the intervening fat involved by the infiltrative lesion can simulate normal adipose tissue whose signal becomes suppressed with fat saturation. If our hypothesis proves to be correct, it might be used as an easy method to discriminate NIPT from NPC. The purpose of this study was to validate our hypothesis to provide a simple and consistent way to differentiate between NIPTs and NPCs on conventional MRI.

Methods

Patients

This study was approved by our institutional review board, and informed consent was waived according to the requirements of a retrospective study.

From January 1997 to December 2014, a search of the electronic medical records and pathology registry of our hospital revealed 21 patients with newly histologically proven NIPT. Although all patients were documented to have undergone MRI studies, seven patients were excluded because of loss of essential MRI data from storage, resulting in 14 patients (9 men, 5 women; age range, 38–87 years; mean, 62 years) who formed the basis of this study. For comparison, we evaluated MRI data of 18 patients (13 men, 5 women; age range, 18–79 years; mean, 44 years) with histologically confirmed NPC that had extended to the infratemporal fossa (T4 stage according to TNM staging system approved by the American Joint Committee on Cancer (16)) from the registry of the Departments of Radiology and Otolaryngology of our hospital between January 2010 and December 2014. We selected these NPC patients, because all patients with NIPT included in the present study demonstrated involvement of the infratemporal fossa on MRI.

Main points

- Aggressive behavior of nasopharyngeal inflammatory pseudotumor (NIPT) frequently makes it difficult to distinguish from nasopharyngeal carcinoma (NPC) both clinically and radiologically.
- Hypointensity on T2-weighted images is an important magnetic resonance imaging feature that can provide a clue to the diagnosis of NIPT and is attributed pathologically to a relative lack of both free water and mobile protons within the fibrotic tissue.
- Compared with NPCs, which usually demonstrate hyperintensity on T2-weighted images, NIPTs usually display hypointensity on T2-weighted images, which can result in less lesion conspicuity and underestimation of the lesion size.
- In our series, compared with NPCs, the size of NIPTs was estimated significantly smaller on fat-suppressed T2-weighted images than on T1-weighted images; discrepancy in the lesion size estimated on T1- and fat-suppressed T2-weighted images may be useful to differentiate between NIPTs and NPCs.

Magnetic resonance imaging

MRI examinations were performed on a 1.5 T or 3.0 T scanner using a head or neurovascular coil. In all patients, unenhanced T1-weighted spin-echo images (TR, 400–560 ms; TE, 10–14 ms; NEX, 2) and T2-weighted fast spin-echo images with fat-suppression (TR, 2500–4500 ms; TE, 80–110 ms; NEX, 1) were obtained, followed by intravenous injection of 0.1 mmol/kg of gadolinium-based contrast material and contrast-enhanced T1-weighted spin-echo images with fat saturation. In all sequences, images were obtained in the axial plane with 3–4 mm section thickness and 0.3–1 mm intersection gap. In addition, images in the sagittal and/or coronal planes were also obtained in most patients.

Image analysis

All MRI data were retrospectively evaluated by two neuroradiologists in consensus, both examiners having experiences with head and neck imaging for 27 years and 7 years, respectively.

For the sake of completeness, we evaluated the MRI data for the general features of NIPTs and NPCs, such as the extent, signal intensity, pattern, and enhancement degree of the lesions, although it was not the main subject of this study. As for the extent, we recorded if the lesion involved the skull base and intracranial cavity in addition to the nasopharynx and infratemporal fossa. We compared the signal intensity of the lesions with that of the brain stem on T1-weighted and fat-suppressed T2-weighted images. On contrast-enhanced MRI, the enhancement pattern of the lesion was classified as homogeneous or heterogeneous. We ranked enhancement degree of the lesion on basis of enhancement of the adjacent muscle: similar to the muscle, mild; greater than the muscle but less than the sinonasal mucosa, moderate; similar to or greater than the sinonasal mucosa, marked.

For measurement of the apparent size of the lesion on images with different pulse sequences, we first obtained A_{CET1} (area of the lesion on contrast-enhanced T1-weighted images) by placing the largest possible manually-drawn polygonal region-of-interest within the lesion on the axial contrast-enhanced T1-weighted image where the area of the lesion involving the infratemporal fossa looked biggest. The infiltrating portions of the lesion at the infratemporal fossa that showed abnormal enhancement were included in the region-of-interest with care to minimize partial volume averaging effect (Figs. 1 and 2). Likewise, for the acquisition of A_{T1} (area of the lesion on unenhanced T1-weighted images) and A_{T2} (area of the lesion on fat-suppressed T2-weighted images), we repeated the process of region-of-interest placement on the axial unenhanced T1-weighted and fat-suppressed T2-weighted images at the same slice as that on the contrast-enhanced T1-weighted images (Figs. 1 and 2). The means and standard deviations of metric data were calculated for A_{CET1}, A_{T1}, and A_{T2}. Based on these measurements, we calculated AR_{T1} (area ratio of T1) and AR_{T2} (area ratio of T2) for each patient, which were determined by the following formulas:

$AR_{T1} = A_{T1}/A_{CET1}$ and $AR_{T2} = A_{T2}/A_{CET1}$

We chose contrast-enhanced T1-weighted imaging as the reference pulse sequence, because NIPTs usually looked biggest and most conspicuous on this sequence, compared with unenhanced T1-weighted and fat-suppressed T2-weighted imaging.

Validation of diagnostic performance and interobserver agreement

To validate the diagnostic performance of our hypothesis, two radiologists (six and five years of experience in neuroradiology, respectively) independently reviewed the MRI data of the same patients enrolled in the present study. Reviewers were unblinded to the clinical indication for MRI, that is, they were aware that the pathology of the lesion was either NIPT or NPC. Otherwise, they were blinded to any other clinical data including the final diagnosis of the individual lesion. Before readings, both reviewers were carefully instructed in the background of the present study and also in our hypothesis that NIPTs would be seen smaller on fat-suppressed T2-weighted images than

Table 1. General MRI features of NIPT and NPC

Diagnosis	Extent[a]		Signal intensity[b]		Pattern of enhancement		Degree of enhancement[c]		
	SB	IC	T1WI	T2WI	Homogeneous	Heterogeneous	Mild	Moderate	Marked
NIPT (n=14)	12	8	Iso, 14	Mixed high/iso/low, 7 Mixed high/low, 6 Mixed iso/low, 1	1	13	-	13	1
NPC (n=18)	8	10	Iso, 18	Mixed high/iso/low, 2 Mixed high/iso, 7 Mixed iso/low, 6 Iso, 3	7	11	-	17	1

[a]All lesions involved both nasopharynx and infratemporal fossa.
[b]Signal intensity of the lesion was compared with that of the brain stem.
[c]Degree of enhancement of the lesion was determined in comparison with the adjacent muscle.
MRI, magnetic resonance imaging; NIPT, nasopharyngeal inflammatory pseudotumor; NPC, nasopharyngeal carcinoma; SB, skull base; IC, intracranial cavity; T1WI, T1-weighted image; T2WI, T2-weighted image.

Table 2. Summary of measurements

Diagnosis	Mean±SD (cm^2)			Median (range)		
	A_{CET1}	A_{T1}	A_{T2}	AR_{T1}	AR_{T2}	P [a]
NIPT (n=14)	6.62±3.92	6.97±3.69	3.35±2.15	1.01 (0.80–1.99)	0.48 (0.18–0.97)	<0.001
NPC (n=18)	10.85±4.97	10.62±4.97	9.59±4.75	0.92 (0.81–1.37)	0.89 (0.67–1.19)	0.08
P [b]				0.149	<0.001	

[a]P value represents AR_{T2} vs. AR_{T1} for NIPT and NPC.
[b]P value represents NIPT vs. NPC for AR_{T1} and AR_{T2}.
SD, standard deviation; A_{CET1}, area of the lesion on contrast-enhanced T1-weighted images; A_{T1}, area of the lesion on unenhanced T1-weighted images; A_{T2}, area of the lesion on fat-suppressed T2-weighted images; AR_{T1}, area ratio of T1; AR_{T2}, area ratio of T2; NIPT, nasopharyngeal inflammatory pseudotumor; NPC, nasopharyngeal carcinoma.

on T1-weighted images before and after contrast enhancement, while NPCs would not. Based on judgment by naked eye, each reviewer made a decision by using a 3-point confidence scale: 1 (suggestive of NIPT), when the lesion size on fat-suppressed T2-weighted images seemed to be less than half of that on T1-weighted images; 2 (suspicious of NIPT), when the lesion size on fat-suppressed T2-weighted images in between scale 1 and 3 compared with that on T1-weighted images; and 3 (suggestive of NPC), when the lesion size on fat-suppressed T2-weighted images are equal to or greater than 90% of that on T1-weighted images. If there was a visual discrepancy in the lesion size between unenhanced and contrast-enhanced T1-weighted images, reviewers were recommended to rely on the latter. Other MRI features known for the diagnosis of NIPT and NPC in the literature were not considered during this validation process.

Statistical analysis

Comparisons between AR_{T1} and AR_{T2} in NIPTs and NPCs were performed using Wilcoxon rank sum test. AR_{T1} and AR_{T2} were compared between NIPTs and NPCs by Mann-Whitney U test. For all tests, $P < 0.05$ was considered statistically significant.

The receiver operating characteristics analysis was undertaken to estimate the diagnostic performance of AR_{T1} and AR_{T2} for differentiating NIPTs from NPCs by achieving the highest Youden index with commercially available software (MedCalc for Windows, version 15.6; MedCalc Software) (17). Scatterplots were established to visualize the distribution of the AR_{T1} and AR_{T2} values of NIPTs and NPCs. With the most relevant cutoff value of AR_{T2} for differentiating NIPTs from NPCs, we calculated the sensitivity, specificity, positive predictive value (PPV), negative predictive value (NPV), and accuracy.

Diagnostic performance for NIPT was evaluated by calculating the sensitivity, specificity, PPV, NPV, and accuracy for each reviewer, with the lesions allotted to a confidence level 1 and 2 being considered as NIPT. Interobserver agreement between the two reviewers was also evaluated by calculating κ statistics. The κ value was categorized in the following way: κ = 0.00–0.20, poor agreement; κ = 0.21–0.40, fair agreement; κ = 0.41–0.60, moderate agreement; κ = 0.61–0.80, good agreement; κ = 0.81–1.00, excellent agreement.

All statistical analyses except for receiver operating characteristics were performed using commercially available software (SPSS, version 22.0.0; IBM Corp.).

Results

The general features of NIPTs and NPCs on conventional MRI are summarized in Table 1. The results of the measurements are summarized in Table 2. In 14 patients with NIPT, the median value of AR_{T2} was 0.48 (range, 0.18–0.97), which was significantly lower than that of AR_{T1} (median, 1.01; range, 0.80–1.99) ($P < 0.001$) (Fig. 1). In contrast, no significant difference was found between AR_{T1} and AR_{T2} in 18 patients with NPC ($P = 0.08$) (Fig. 2). While AR_{T1} of NIPT was not statistically different from that of NPC ($P = 0.149$), AR_{T2} of NIPT was significantly lower than that of NPC ($P < 0.001$).

Using AR_{T2} for the prediction of NIPTs, the mean area under the receiver operating characteristics curve was 0.933 (95% confidence interval, 0.79–0.99). With 0.69 AR_{T2} as the cutoff value for differentiating NIPTs from NPCs, the sensitivity, specificity, PPV, NPV, and accuracy were 86% (12/14), 94% (17/18), 92% (12/13), 89% (17/19), and 91% (29/32), respectively. There were two false negative cases (i.e., NIPT with $AR_{T2} > 0.69$; Fig. 3) and one false positive case (i.e., NPC with $AR_{T2} < 0.69$; Fig. 4). A scatterplot is presented in Fig. 5 to demonstrate these results.

We summarized the results of interpretation by two reviewers in Table 3. Based on

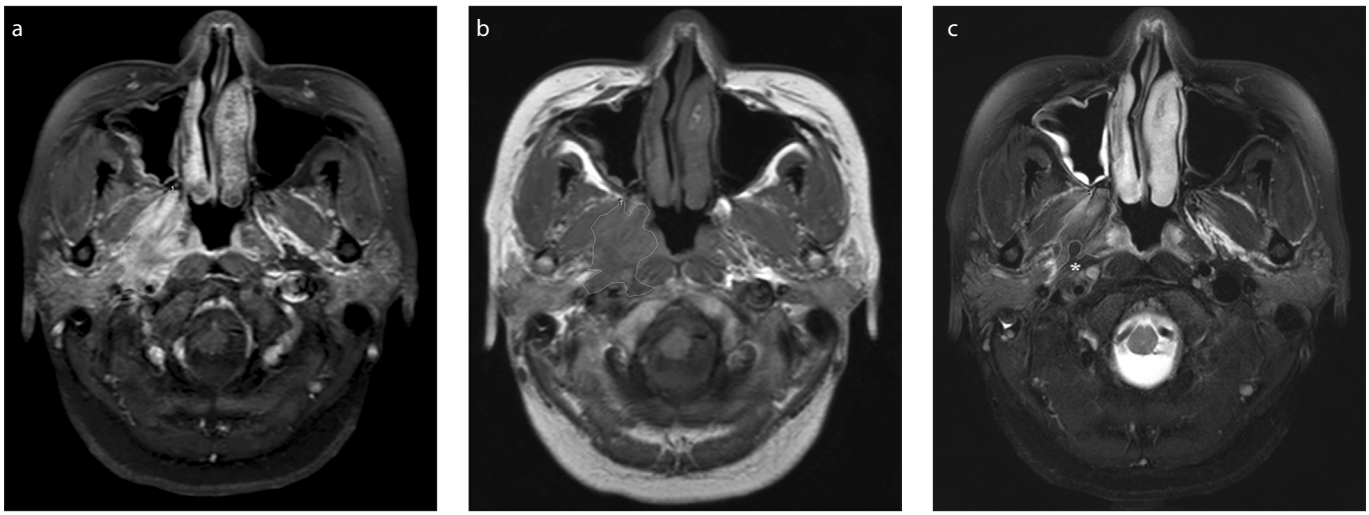

Figure 1. a–c. A representative case of nasopharyngeal inflammatory pseudotumor (NIPT). Axial contrast-enhanced **(a)** and unenhanced **(b)** T1-weighted images show an ill-defined, heterogeneously well-enhancing mass in the right infratemporal fossa. Axial fat-suppressed T2-weighted image **(c)** shows heterogeneous signal intensity of the mass. The low signal intensity in the posterior part of the lesion *(**c**, asterisk)*, which is similar to the adjacent prevertebral muscle, results in underestimation of the size of the lesion. The AR_{T1} and AR_{T2} in this case were 0.90 and 0.66, respectively.

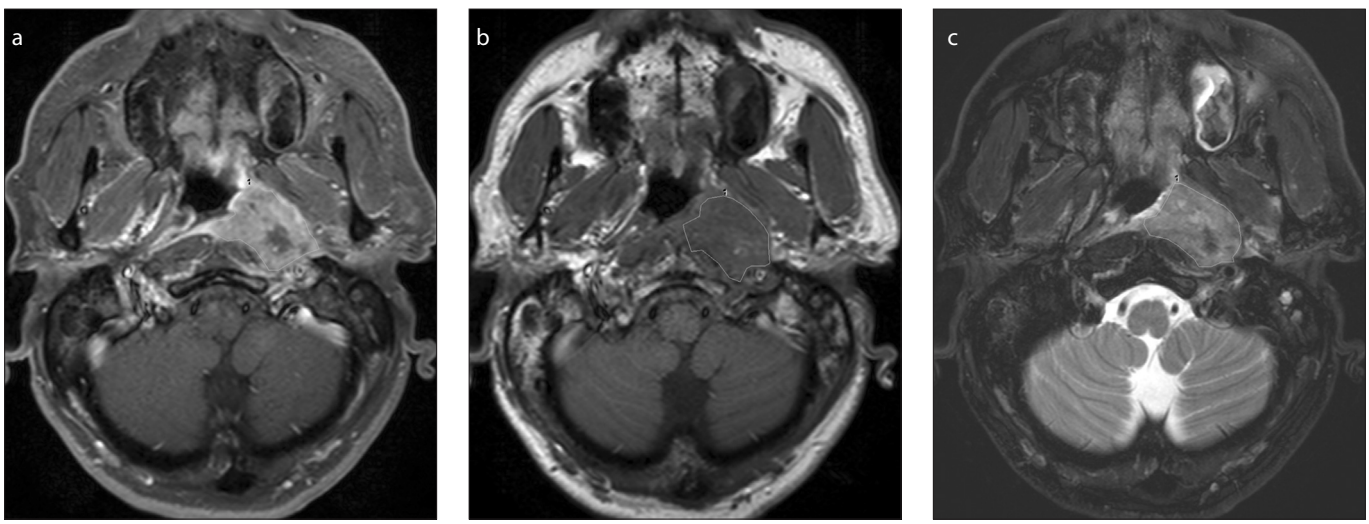

Figure 2. a–c. A representative case of nasopharyngeal carcinoma (NPC). Axial contrast-enhanced **(a)** and unenhanced **(b)** T1-weighted images show an ill-defined, heterogeneously enhancing mass in the nasopharynx and infratemporal fossa on the left. Axial fat-suppressed T2-weighted image **(c)** shows heterogeneous signal intensity of the mass, which is hyperintense to the adjacent muscle. The AR_{T1} and AR_{T2} in this case were 0.90 and 0.95, respectively.

Table 3. Diagnostic performance of the two reviewers

	Diagnosis of Reviewer 1		Diagnosis of Reviewer 2	
Histologic diagnosis	NIPT	NPC	NIPT	NPC
NIPT (n=14)	13	1	13	1
NPC (n=18)	1	17	3	15

Reviewer 1: 93% sensitivity, 94% specificity, 93% positive predictive value (PPV), 94% negative predictive value (NPV), 94% accuracy.
Reviewer 2: 93% sensitivity, 83% specificity, 81% PPV, 93% NPV, 88% accuracy.
NIPT, nasopharyngeal inflammatory pseudotumor; NPC, nasopharyngeal carcinoma.

their visual inspection, interpretations of reviewer 1 had 93% (13/14) sensitivity, 94% (17/18) specificity, 93% (13/14) PPV, 94% (17/18) NPV, 94% (30/32) accuracy; interpretations of reviewer 2 had 93% (13/14) sensitivity, 83% (15/18) specificity, 81% (13/16) PPV, 93% (15/16) NPV, and 88% (28/32) accuracy. There were one false negative case (Fig. 3) and one false positive case (Fig. 4) in reviewer 1, and one false negative case and three false positive cases in reviewer 2. The two cases misinterpreted by reviewer 1 were also misinterpreted by reviewer 2. The interobserver agreement for differentiation between NIPT and NPC was good with a κ value of 0.75.

Discussion

IPT is an idiopathic, quasi-neoplastic disease and can manifest as a single mass or multiple masses. It is characterized histologically by polymorphous infiltration of both acute and chronic inflammatory cells, including lymphocytes, plasma cells, histiocytes, and eosinophils with variable amounts of fibrosis, granulomatous reaction, necrosis, and myofibroblastic spindle cells (1, 2,

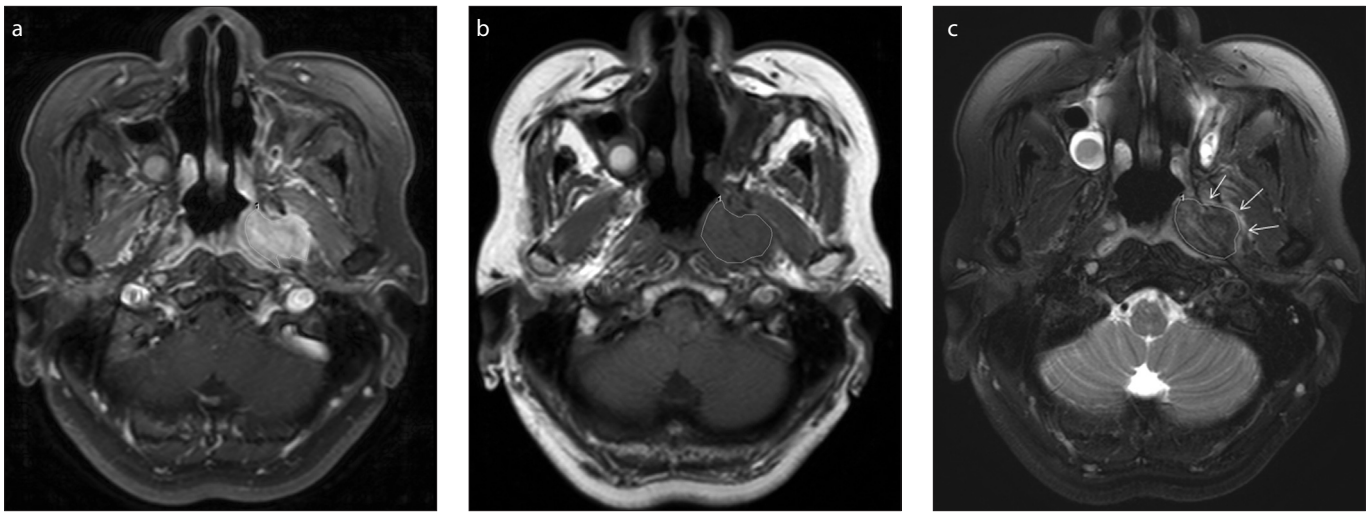

Figure 3. a–c. A false negative case. Axial contrast-enhanced **(a)** and unenhanced **(b)** T1-weighted images show an ill-defined, heterogeneously enhancing mass in the left infratemporal fossa. Axial fat-suppressed T2-weighted image **(c)** shows the mass principally composed of hypointensity, comparable to the adjacent muscle. However, the peripheral rind of curvilinear hyperintensity surrounding the mass *(arrows)*, which probably represents perilesional edema, leads us to draw the region-of-interest along it, resulting in no significant difference in the area measurements between A_{CET1} and A_{T2}. The AR_{T1} and AR_{T2} in this case were 1.02 and 0.97, respectively. Both reviewers scored 3 for this lesion in favor of NPC. The lesion proved to be NIPT on histologic examination.

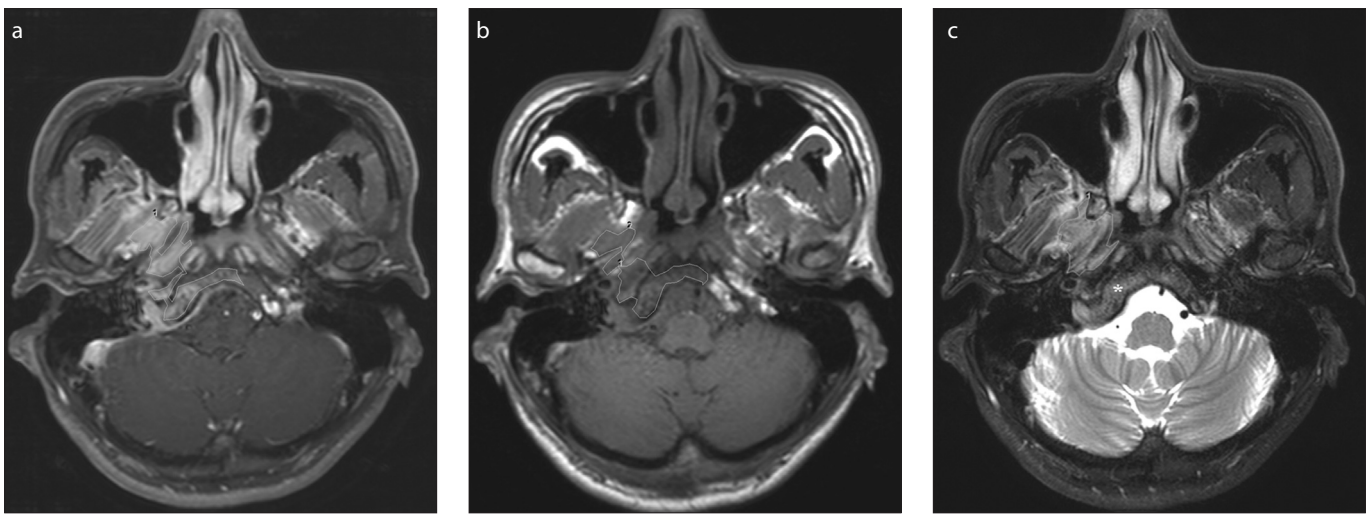

Figure 4. a–c. A false positive case. Axial contrast-enhanced **(a)** and unenhanced **(b)** T1-weighted images show an ill-defined, heterogeneously enhancing mass in the nasopharynx, skull base, and infratemporal fossa on the right. Axial fat-suppressed T2-weighted image **(c)** shows apparent hyperintensity of the mass in the infratemporal fossa. However, the signal intensity of the lesion in the clivus *(asterisk)* is indistinguishable from the unaffected portion of the clivus, resulting in underestimation of the size of the lesion on this fat-suppressed T2-weighted image. The AR_{T1} and AR_{T2} in this case were 0.91 and 0.67, respectively. The two reviewers scored 1 and 2 for this lesion, respectively, both in favor of NIPT. The lesion proved to be NPC on histologic examination.

18–21). Since its first observation in the lung in 1939, many different terms have been coined to describe IPT, such as inflammatory myofibroblastic tumor, plasma cell granuloma, inflammatory myofibrohistiocytic proliferation, inflammatory fibrosarcoma, xanthoma, xanthogranuloma, fibroxanthoma, histiocytoma, xanthomatous pseudotumor, plasmocytoma, and solitary mast cell granuloma, indicating the complex and diverse nature of this entity (1). Although the lung and the orbit are two most common sites involved by IPT, the disease can occur in nearly every site of the body (1, 18).

The imaging findings of IPT are nonspecific and variable depending on the anatomic locations and pathologic composition of the lesions. Pulmonary IPT typically presents as a solitary, peripheral, well-demarcated lobulated mass with a predilection for the lower lobes (22) and shows intermediate signal intensity on T1-weighted images and high signal intensity on T2-weighted images (23). On the other hand, orbital IPT can be localized or diffuse and shows hypointense signal intensity on both T1- and T2-weighted images (24–27). Recent systemic reviews on IPTs of the sinonasal cavity and skull base reported that compared with gray matter, the majority of the lesions demonstrated isointensity on T1-weighted images and hypointensity on T2-weighted images along with confluent and homogeneous contrast enhancement (28, 29).

Although rare, NIPT has similar MRI findings (2, 3, 5). In their study of seven patients with NIPT, Lu et al. (2) reported that an infiltrative nature, minimal-to-mild mass effect, low signal intensity on T2-weighted images, and moderate homogeneous contrast enhancement were the characteristic MRI findings of NIPT that were useful for

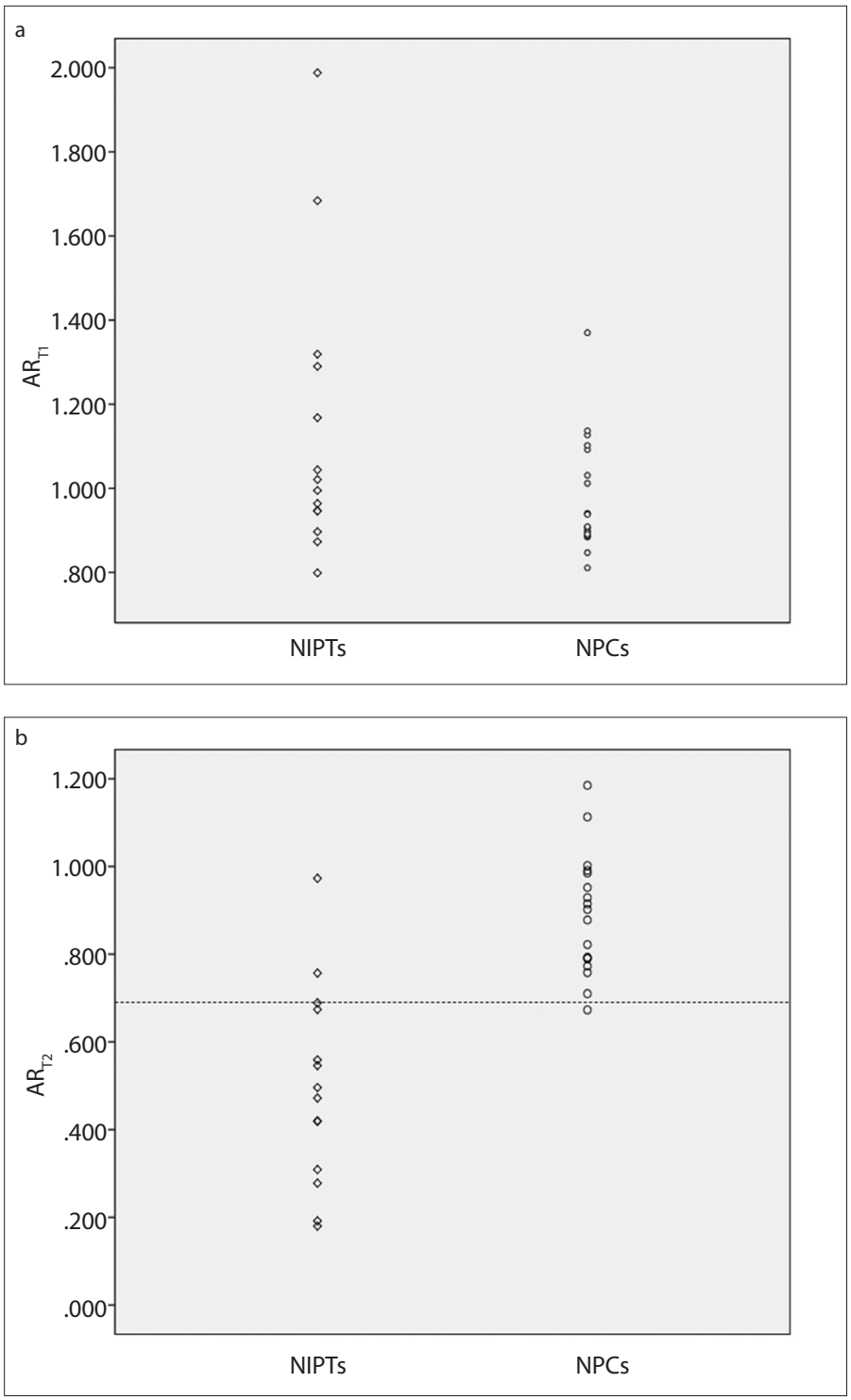

Figure 5. a, b. Scatterplots displaying the various values of AR_{T1} **(a)** and AR_{T2} **(b)** in NIPTs and NPCs. While there is no reliable cutoff value of AR_{T1} for differentiation between the two groups, with AR_{T2} cutoff set at 0.69, NIPTs can be differentiated from NPCs with 86% sensitivity, 94% specificity, 92% PPV, 89% NPV, and 91% accuracy.

differential diagnosis of NPC. Our study also revealed similar findings in most patients with NIPT. Lu et al. (2) also reported that intact mucosa of nasopharynx, extensive pachymeningeal involvement, encircling and narrowing of internal carotid artery and a relative lack of associated cervical lymphadenopathy were additional MRI findings in favor of NIPT. Of the MRI features, hypointensity on T2-weighted images is known as the most important clue to the diagnosis of IPT (2, 3, 9). This hypointensity on T2-weighted images is attributed pathologically to a relative paucity of free water as well as mobile protons in fibrotic tissues.

The results of the present study support our hypothesis that hypointensity of NIPT causes less lesion conspicuity and underestimation of the lesion size on fat-suppressed T2-weighted images, while this does not happen in cases of NPC. As expected, not only the internal low signal intensity but also the infiltrative growth pattern frequently obscured the boundary of the lesion, resulting in a decreased AR_{T2} in NIPT compared with NPC. We validated our hypothesis by the use of the receiver operating characteristics analysis and scatterplots as well as in a double-blinded study by two reviewers. With the cutoff value of 0.69 AR_{T2}, we achieved a sensitivity of 86% and a specificity of 94%. The validation study by two reviewers based on visual inspection also revealed a sensitivity of 93% and a specificity of 83%–94%. Although there were exceptions of false negative and false positive cases, the present study shows that recognition of discrepant lesion size on T1- and fat-suppressed T2-weighted images can afford a simple but consistent way to differentiate between NIPTs and NPCs.

Our study has several limitations. First, it is retrospective in nature and thus might have an inherent selection bias. Second, this study included only a limited number of patients with NIPT. Third, the placement of the region-of-interests on magnetic resonance images might not be exact, because the boundary of the lesion was not certain in some cases. However, the results of the blinded qualitative validation study, which were similar to the results of the quantitative study, indicate that this may not matter in most cases. Fourth, there is lack of correlation between pathologic specimens and images. Intra-tumor microcalcification, hemorrhage, or other T2* change such as macrophage and free radical of NIPT may be related to relative low signal intensity on T2-weighted images.

In conclusion, in contrast to NPCs, NIPTs appear smaller on fat-suppressed T2-weighted images than on T1-weighted images. This discrepancy in the lesion size estimated on T1- and fat-suppressed T2-weighted images may be useful to differentiate between NIPTs and NPCs.

Conflict of interest disclosure

The authors declared no conflicts of interest.

References

1. Narla LD, Newman B, Spottswood SS, Narla S, Kolli R. Inflammatory pseudotumor. Radiographics 2003; 23:719–729. [CrossRef]
2. Lu CH, Yang CY, Wang CP, Yang CC, Liu HM, Chen YF. Imaging of nasopharyngeal inflammatory pseudotumours: differential from nasopharyngeal carcinoma. Br J Radiol 2010; 83:8–16. [CrossRef]
3. Choi SY, Yu IK, Han MH, Lee BH, Song CJ, Kim KS. Fibrosing inflammatory pseudotumor of the nasopharynx: MR features and histopathologic correlation. Eur J Radiol 2009; 72:274–277. [CrossRef]
4. Chwang WB, Jain R, Narayan A, et al. Inflammatory pseudotumor of the nasopharynx and skull base: mimicking an aggressive neoplasm or infection. Arch Otolaryngol Head Neck Surg 2012; 138:765–769. [CrossRef]
5. Hildenbrand P, Temin NN, Catalano PJ, Dolan RW. Nasopharyngeal inflammatory pseudotumor: multimodality imaging characterization. Eur J Radiol 2009; 72:e61–e64. [CrossRef]
6. Cho KS, Kim HJ, Lee CH, Roh HJ. Nasopharyngeal inflammatory pseudotumor showing abducens nerve palsy. Auris Nasus Larynx 2011; 38:543–546. [CrossRef]
7. Gadde J, Franck B, Liu X, Teixido M, Rizk H. Inflammatory pseudotumor of the nasopharynx with spread along the trigeminal nerve. Am J Otolaryngol 2013; 34:252–254. [CrossRef]
8. Lee DK, Cho YS, Hong SH, Chung WH, Ahn YC. Inflammatory pseudotumor involving the skull base: response to steroid and radiation therapy. Otolaryngol Head Neck Surg 2006; 135:144–148. [CrossRef]
9. Han MH, Chi JG, Kim MS, et al. Fibrosing inflammatory pseudotumors involving the skull base: MR and CT manifestations with histopathologic comparison. AJNR Am J Neuroradiol 1996; 17:515–521.
10. McKinney AM, Short J, Lucato L, SantaCruz K, McKinney Z, Kim Y. Inflammatory myofibroblastic tumor of the orbit with associated enhancement of the meninges and multiple cranial nerves. AJNR Am J Neuroradiol 2006; 27:2217–2220.
11. Chen JM, Moll C, Schotton JC, Fisch U. Inflammatory pseudotumors of the skull base. Skull Base Surg 1994; 4:93–98. [CrossRef]
12. Weber MA, Viehoever A, Stieltjes B, et al. Intracerebral manifestation of an atypical monoclonal plasma cell hyperplasia depicted by MR perfusion and diffusion tensor imaging and MR spectroscopy. AJR Am J Roentgenol 2005; 185:784–787. [CrossRef]
13. Krouwer HG, Kim TA, Rand SD, et al. Single-voxel proton MR spectroscopy of nonneoplastic brain lesions suggestive of a neoplasm. AJNR Am J Neuroradiol 1998; 19:1695–1703.
14. Kapur R, Sepahdari AR, Mafee MF, et al. MR imaging of orbital inflammatory syndrome, orbital cellulitis, and orbital lymphoid lesions: the role of diffusion-weighted imaging. AJNR Am J Neuroradiol 2009; 30:64–70. [CrossRef]
15. Ginat DT, Bokhari A, Bhatt S, Dogra V. Inflammatory pseudotumors of the head and neck in pathology-proven cases. J Neuroradiol 2012; 39:110–115. [CrossRef]
16. Edge SB, Byrd DR, Compton CC, Fritz AG, Greene FL, Trotti A. AJCC cancer staging manual. 7th ed. New York: Springer-Verlag, 2010; 41–56.
17. Youden WJ. Index for rating diagnostic tests. Cancer 1950; 3:32–35.
18. Patnana M, Sevrukov AB, Elsayes KM, Viswanathan C, Lubner M, Menias CO. Inflammatory pseudotumor: the great mimicker. AJR Am J Roentgenol 2012; 198:W217–227. [CrossRef]
19. Hedlund GL, Navoy JF, Galliani CA, Johnson WH, Jr. Aggressive manifestations of inflammatory pulmonary pseudotumor in children. Pediatr Radiol 1999; 29:112–116. [CrossRef]
20. Safran D, Welch J, Rezuke W. Inflammatory pseudotumors of the spleen. Arch Surg 1991; 126:904–908. [CrossRef]
21. Scott L, Blair G, Taylor G, Dimmick J, Fraser G. Inflammatory pseudotumors in children. J Pediatr Surg 1988; 23:755–758. [CrossRef]
22. Agrons GA, Rosado-de-Christenson ML, Kirejczyk WM, Conran RM, Stocker JT. Pulmonary inflammatory pseudotumor: radiologic features. Radiology 1998; 206:511–518. [CrossRef]
23. Patankar T, Prasad S, Shenoy A, Rathod K. Pulmonary inflammatory pseudotumour in children. Australas Radiol 2000; 44:318–320. [CrossRef]
24. Mendenhall WM, Lessner AM. Orbital pseudotumor. Am J Clin Oncol 2010; 33:304–306.
25. Ohtsuka K, Hashimoto M, Suzuki Y. A review of 244 orbital tumors in Japanese patients during a 21-year period: origins and locations. Jpn J Ophthalmol 2005; 49:49–55. [CrossRef]
26. Smitt MC, Donaldson SS. Radiation therapy for benign disease of the orbit. Semin Radiat Oncol 1999; 9:179–189. [CrossRef]
27. Park SB, Lee JH, Weon YC. Imaging findings of head and neck inflammatory pseudotumor. AJR Am J Roentgenol 2009; 193:1180–1186. [CrossRef]
28. Desai SV, Spinazzi EF, Fang CH, et al. Sinonasal and ventral skull base inflammatory pseudotumor: a systematic review. Laryngoscope 2015; 125:813–821. [CrossRef]
29. Spinazzi EF, Desai SV, Fang CH, et al. Lateral skull base inflammatory pseudotumor: A systematic review. Laryngoscope 2015; 125:2593–2600. [CrossRef]